BIOCHEMISTRY
including biophysical chemistry & molecular biology

Article

pubs.acs.org/biochemistry

Zinc Modulates Self-Assembly of *Bacillus thermocatenulatus* Lipase

Emel Timucin* and O. Ugur Sezerman

Sabanci University, Faculty of Engineering and Natural Sciences, Molecular Biology, Genetics and Bioengineering, 34956 Istanbul, Turkey

Supporting Information

ABSTRACT: Thermoalkalophilic lipases are prone to aggregation from their dimer interface to which structural zinc is very closely located. Structural zinc sites have been shown to induce protein aggregation, but the interaction between zinc and aggregation tendency in thermoalkalophilic lipases remains elusive. Here we delineate the interplay between zinc and aggregation of the lipase from *Bacillus thermocatenulatus* (BTL2), which is taken to be a representative of thermoalkalophilic lipase. Results showed that zinc removal disrupted the BTL2 dimer, leading to monomer formation and reduced thermostability manifesting as a link between zinc and dimerization that leads to thermostability, while zinc addition induced aggregation. Biochemical and kinetic characterizations of zinc-induced aggregates showed that the aggregates obtained from the early and late stages of aggregation had differential characteristics. In the early stages, the aggregates were soluble and possessed native-like structures, while in the late stages, the aggregates became insoluble and showed fibrillar characteristics with binding affinities for Congo red and thioflavin T. The impact of temperature on zinc-induced aggregation was further investigated, and it was found that the native-like early aggregates could completely dissociate into functional lipase forms at high temperatures while dissociation of the late aggregates was limited. To this end, we report that the zinc-induced aggregation of BTL2 can be reversed by temperature switches and initiated by ordered aggregates in the early stages that gain fibrillar-like features over time. Insights revealed by this work contributes to the knowledge of aggregation mechanisms that exist in thermophilic proteins, reflecting the potential use of metal addition and/or removal to fine-tune aggregation tendency.

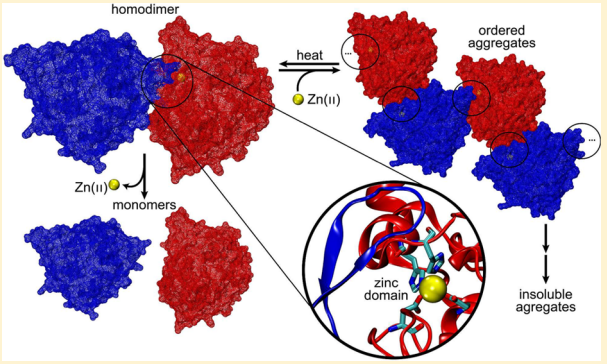

Bacterial thermoalkalophilic lipases grouped in lipase family I.5 have sequences that are 90% identical with each other, while their sequences are only 30% identical with those of other lipases. Despite the fact that these lipases offer robust alternatives to chemical transformations with ability to resist the harsh conditions of industrial processes,[1] they are prone to aggregation,[2−5] which is a major concern for industrial enzymes. So far, numerous efforts have been devoted to understanding aggregation processes that might decrease the solubility of potentially important bioproducts and thus result in loss of yield during industrial applications.[6,7] Hence, identification of the factors leading to aggregation of thermoalkalophilic lipases is critical not only to the design of novel lipase variants with optimal solubility but also to the theoretical description of the main principles behind aggregation processes that have also been linked to neurodegenerative diseases affecting humans.[8−10] Such efforts remain a recurrent issue in science, medicine, and biotechnological areas.

Aggregation tendency is a well-documented feature of many lipases,[11−13] for most of which a high content of hydrophobic amino acids is identified as the leading cause of aggregation.[11,14−16] On the other hand, aggregation tendency of the thermoalkalophilic lipase originating from *Bacillus thermocatenulatus* (BTL2) cannot be explained by this criteria because of the relatively lower hydrophobic content of BTL2 compared to those of other aggregation-prone lipases.[4] Along with this information, the evolutionary isolation of thermoalkalophilic lipases from other families reinforces the necessity of inspecting the factors contributing to the aggregation of thermoalkalophilic lipases with different rigor.

Despite the fact that the underlying mechanism of aggregation in thermoalkalophilic lipases remains elusive, their natural aggregation tendency has been investigated thoroughly.[4,5,17,18] In these studies, Rua et al.[4] and Salameh et al.[18] have found that detergent-like molecules that were able to dissolve aggregates enhance the activity of thermoalkalophilic lipase aggregates by increasing the number of available active sites. Their findings, showing that the aggregates dissociate into functional lipase forms, essentially imply that thermoalkalophilic lipases are prone to aggregation at their native states. The particular capacity of these lipase aggregates to break into functional forms, analogous to true biochemically defined

Received: February 26, 2015
Revised: May 26, 2015
Published: June 9, 2015

DOI: 10.1021/acs.biochem.5b00200
Biochemistry 2015, 54, 3901−3910

oligomers, accentuates the oligomeric structures of BTL2 for investigation of the aggregation process.

Inspection of the structures belonging to thermoalkalophilic lipases found in the Protein Data Bank (PDB) revealed that, when crystallization was performed in the absence of any substrate analogue, thermoalkalophilic lipases adopted a homodimeric form (PDB entries 1KU0,[19] 1JI3,[20] 2DSN,[21] and 3UMJ[22]). Upon investigation of these dimer structures, an identical subunit interface for all of the structures has been spotted. This unique interface was shown to be contoured by the asymmetric portions of the lipase monomers. The tendency of asymmetric subunit portions to contour the binding interface provides the homodimer with two additional faces for higher levels of oligomer formation. Therefore, in theory, the dimer can grow to higher-order oligomeric forms and/or native-like aggregates through the unique interface resolved in crystal structures. In line with this notion, a recent study has shown through mutagenesis studies that the disruption of the dimer interactions has been shown to inhibit aggregation of BTL2,[17] rendering the dimer interface extremely important for deciphering the details of the aggregation mechanism allocated by thermoalkalophilic lipases.

Although structural zinc sites are very rare in lipases,[23] succinct investigation of the unique dimer interface reveals that thermoalkalophilic lipases possess a zinc coordination site that is very close to the dimer interface. The proximity of zinc to the dimer interface that has been shown to be employed in the aggregation of BTL2[17] implied that zinc might be involved in mediating intermolecular interactions during aggregation. Moreover, considering that divalent metals such as zinc have been previously associated with native-like aggregation mechanisms,[24−30] it is evident that identification of the interplay between zinc and aggregation tendency is crucial for a complete understanding of the self-assembly process of thermoalkalophilic lipases.

Aggregation can be studied under various conditions such as incubation at acidic pH,[31] altered proteolysis,[32] and divalent metal incubations.[26−30] In this study, we were particularly interested in zinc-induced aggregation of the thermoalkalophilic lipase BTL2. We have investigated the impact of the presence and absence of zinc on the oligomeric state of BTL2 and explored the biochemical and biophysical characteristics of zinc-induced aggregates. We also analyzed the effect of temperature on the zinc-induced aggregates in CD experiments and enzymatic assays. Lastly, we used previously identified structural data of thermoalkalophilic lipases to address a molecular basis of zinc-induced oligomerization.

MATERIALS AND METHODS

Lipase Expression and Purification. *Escherichia coli* SHuffle cells (New England Biolabs) were transformed with expression plasmid pMCSG7 (DNASU plasmid repository) carrying the 1167 bp DNA fragment corresponding to the mature BTL2 gene. BTL2 was expressed in *E. coli* cells that were cultivated in Luria-Bertani medium (low-salt formulation) supplemented with 100 μg/mL ampicillin and with 1 mM isopropyl β-D-thiogalactopyranoside for induction. Expression was continued for 4 h at 37 °C, and subsequent purification of BTL2 was conducted as described previously[33] using HisTrap HP columns (GE Healthcare Life Sciences) by the availability of an N-terminal polyhistidine tag. The protein concentration was determined using a Bradford assay, and the purity of the recombinant lipase was tested by sodium dodecyl sulfate−polyacrylamide gel electrophoresis (SDS−PAGE).

Preparation of Aggregates and Zinc-Free BTL2. Zinc-induced aggregates were prepared in a consistent manner for all of the experiments. Recombinant BTL2 was diluted to 10 μM (0.43 mg/mL) in 10 mM HEPES-KOH buffer (pH 7.4) unless otherwise stated and incubated at varying zinc concentrations for 2 h at room temperature. The control sample was incubated under the same conditions without any zinc addition. Zinc-free BTL2 was prepared as described previously;[34] 100 μM lipase samples were incubated in 10 mM sodium phosphate buffer (pH 7.4) and 2 μM *N*,*N*,*N*′,*N*′-tetrakis(2-pyridylmethyl)-ethylenediamine (TPEN) for 12 h at 4 °C and then dialyzed against 10 mM sodium phosphate buffer (pH 7.4) to remove unbound TPEN and/or TPEN−Zn^{2+} complexes. The zinc-free BTL2 concentration was set to 10 μM. During preparation of zinc-free BTL2, all of the buffers were treated with 0.2 g/mL Chelex (Sigma) at room temperature for 2 h.

Dynamic Light Scattering. Samples containing 10 μM lipases in 10 mM HEPES-KOH buffer (pH 7.4) were incubated at varying concentrations of zinc for 2 h and filtered (0.22 μm) prior to measurements. Dynamic light scattering (DLS) was conducted using Zetasizer NanoXS (Malvern Instruments) at 25 °C and repeated three times. Although the size distribution generated by DLS is an intensity distribution, it was converted to volume distribution using Mie's theory.[35] This conversion was performed via the Zetasizer software.

Circular Dichroism Spectroscopy. Far-UV circular dichroism (CD) spectra of the same samples were recorded with a 1.0 mm path length using a J-815 spectropolarimeter (Jasco) in a N_2 atmosphere equipped with a thermostatically controlled cuvette at a scanning speed of 100 nm/min. Three scans were averaged to obtain the final spectra that were corrected for background. The mean residue ellipticity (MRE) $[\theta]$ is calculated with the equation

$$[\theta] = \theta M/(10cln_R)$$

where θ is the observed ellipticity in millidegrees, M is the molecular mass in grams per mole, c is the concentration in milligrams per milliliter, l is the cell length in centimeters, and n_R is the number of residues. Thermal denaturation profiles were determined by tracing the 222 nm signal at a heating rate of 6 °C/min from 30 to 90 °C. Melting temperature (T_m) values were calculated from the midpoint of the transition curves between folded and unfolded states of the lipases. Time course measurements were conducted every second for 2 h. CD data were not corrected for the zinc-induced aggregates but given in ellipticity because of excess light scattering from the aggregates.

Congo Red Binding Assays. A volume of 100 μL of 10 μM lipase in 10 mM HEPES-KOH buffer (pH 7.4) was mixed with 400 μL of 20 μM Congo red in 5 mM phosphate buffer and 150 mM NaCl (pH 7.4).[36] The absorption spectra were recorded from 425 to 700 nm using a UV-3600 UV−visible spectrophotometer (Shimadzu). The differential spectra were recorded by subtracting only Congo red and only lipase spectra from the spectrum of the Congo red with lipase preincubated with zinc. For all measurements, 5 mM phosphate buffer and 150 mM NaCl (pH 7.4) were used as a reference.

Thioflavin T Fluorescence Assay. The aggregates formed upon incubation of 10 μM BTL2 at the indicated zinc concentrations for 2 h were mixed with 400 μL of 20 μM thioflavin T (ThT) and 10 mM phosphate buffer (pH 7.4). The

DOI: 10.1021/acs.biochem.5b00200
Biochemistry 2015, 54, 3901−3910

fluorescence of the resulting samples was measured at 25 °C using a Gemini XS (Molecular Devices) spectrofluorimeter. The excitation and emission wavelengths were 440 and 485 nm, respectively.[37]

Lipase Activity Assays. Enzyme assays were performed with 4-methylumberrylferyl (4-MU) caprylate as the substrate in 10 mM phosphate buffer (pH 7.4) in a kinetic fashion. Gemini XS (Molecular Devices) was used to measure 4-MU fluorescence with excitation at 355 nm and emission at 460 nm. The assays were conducted at room temperature using 5 nm of lipase in the final reaction mixture. The percent residual activity was calculated by setting the rate of the control sample without any incubation to 100%. All of the assays were repeated at least three times to test for reproducibility.

Gel Electrophoresis. Aggregation was induced by either 20 or 50 μM zinc and at either 25 or 60 °C. The mixtures were sampled before zinc addition and every 30 min for 2 h after zinc addition. The soluble fractions were obtained by centrifugation at 13000 rpm for 30 min. Before gel loading, total and soluble fractions were mixed with SDS sample buffer and boiled for 5 min. The samples were run on a 12% polyacrylamide gel for 2 h at 100 V and stained with Coomassie blue.

Structural Investigations. We selected the thermoalkalophilic lipase from *Bacillus stearothermophilus* (PDB entry 1KU0) for structural investigations because there was not any structure in the absence of a substrate analogue belonging to BTL2. The illustrations were obtained by using visual molecular dynamics (VMD)[38] with a special focus on the zinc site and the subunit interface of the dimer.

RESULTS

Effect of Zinc on the Size of BTL2. BTL2 was incubated at zinc concentrations ranging from 0 to 100 μM and analyzed by DLS. Figure 1 shows the size distributions by volume. The recombinant BTL2 yielded a 7 nm peak that became aggregated with sizes that grew gradually larger upon incubation with an increasing zinc concentration (Figure 1). On the other hand, the zinc-free BTL2 had a radius of ~3.5 nm (Figure 1).

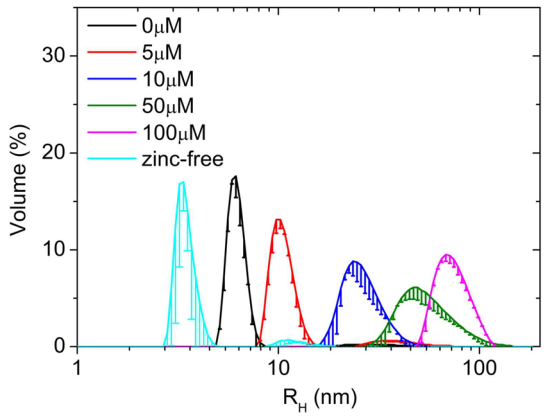

Figure 1. Size distributions of BTL2 by volume. BTL2 was incubated for 2 h at the indicated zinc concentrations that were represented by different colors: black, 0 μM; red, 5 μM; blue, 10 μM; green, 50 μM; pink, 100 μM; cyan, zinc-free BTL2 that was treated with TPEN. Error bars represent standard deviations obtained from three measurements.

Effect of Zinc on the Secondary Structure. The far-UV CD spectra of the samples used in DLS experiments are shown in Figure 2. The native BTL2 yielded two minimal peaks at 208 and 222 nm (Figure 2). Although incubation of BTL2 in 5 μM zinc displayed a far-UV CD spectrum similar to that of native BTL2, incubation conditions of 10, 50, and 100 μM zinc resulted in a loss of the native far-UV signals, with the one around 208 nm being the most significant (Figure 2). When zinc was chelated, the far-UV spectrum of the zinc-free BTL2 only slightly differed from that of native BTL2 (Figure 2).

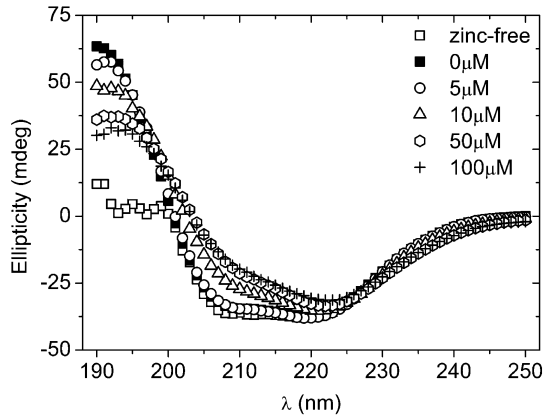

Figure 2. Far-UV CD spectra. The CD spectra of the lipases at 10 μm incubated with (■) 0, (○) 5, (△) 10, (◇) 50, and (+) 100 μM zinc and (□) zinc-free BTL2 are shown after subtraction of the buffer-only spectrum, but without MRE conversions due to excess light scattering from the aggregates. Refer to the Supporting Information (Figure S9) for the reports of MRE of control and zinc-free BTL2.

Dye Binding Characteristics of the Zinc-Induced Aggregates. The samples incubated at various zinc concentrations were analyzed through binding assays of specific dyes as indicators of ordered aggregates.[36,39] The dye, Congo red, gave a maximal absorption at 490 nm (Figure 3A). Although the absorption maximum of Congo red with BTL2 was also located at 490 nm, it gave higher absorption for every wavelength compared with the spectrum of only Congo red (Figure 3A), a result highly likely to be due to the presence of protein. After incubation of BTL2 at ≥20 μM zinc, we observed a peak around 540 nm (Figure 3B), suggesting ordered aggregates in those samples. The same samples were also stained with ThT to further assess the presence of ordered aggregates (Figure 3C). The samples incubated in the presence of low zinc concentrations did not show any significant increase in ThT fluorescence, while samples incubated at zinc concentrations in the range of 50−100 μM produced a 4-fold increase in ThT fluorescence (Figure 3C). The aggregates formed at 50 μM zinc were also examined under a fluorescence microscope, and Figure S1 of the Supporting Information shows the micrographs of the aggregates emitting ThT fluorescence. Overall dye binding analyses suggested that the zinc-induced aggregates that formed at ≥20 μM zinc possessed binding affinities for both Congo red and ThT.

Kinetic Analysis of Zinc-Induced Aggregation. The far-UV CD spectra confirmed that zinc-induced aggregation led to a reduction in ellipticity at 208 nm (Figure 2). To probe the kinetics of zinc-induced aggregation, we relied on this CD spectroscopic change and measured the changes in the CD signal at 208 nm for 2 h upon addition of zinc. Despite the observation that the zinc-induced aggregates also led a reduction in the magnitude of the CD signal at 222 nm

DOI: 10.1021/acs.biochem.5b00200
Biochemistry 2015, 54, 3901−3910

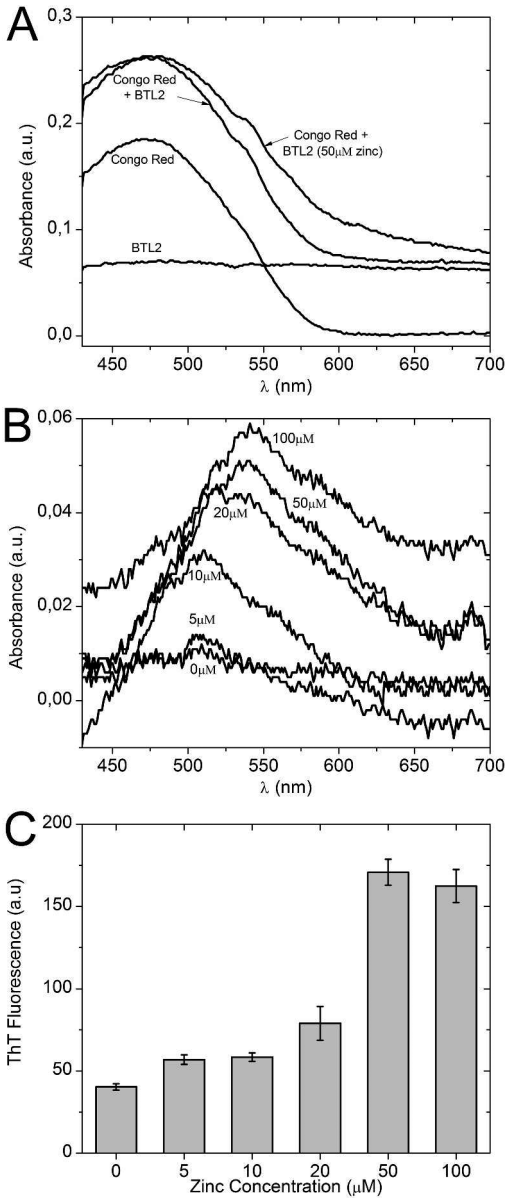

Figure 3. Dye binding analysis of zinc-induced aggregates. (A) Absorption spectra of Congo red only, BTL2 only, BTL2 with Congo red, and BTL2 incubated at 50 μM zinc with Congo red. (B) Spectral difference of the incubations at different zinc concentrations in the range of 0−100 μM from the spectra of lipase only and Congo red only. (C) ThT fluorescence obtained from the same samples analyzed in panel B measured using excitation at 440 nm and emission at 485 nm. The error bars represent standard deviations from two independent experiments.

(Figure 2), CD spectroscopic changes at 222 nm were not sufficient to unveil the impacts of varying zinc concentrations on the rate of aggregation. Hence, for kinetic analysis, we used the 208 nm signal for which we observed a scattering larger than, i.e., a larger reduction in CD intensity, that at 222 nm, allowing us to monitor aggregation rates at varying zinc concentrations.

Table SI of the Supporting Information lists the rate constants of the process that were calculated using linear or exponential fits of the CD data. BTL2 in the presence of 0 μM zinc did not show any changes in ellipticity at 25 °C (Figure 4A). Although the addition of 10 μM zinc did not make any

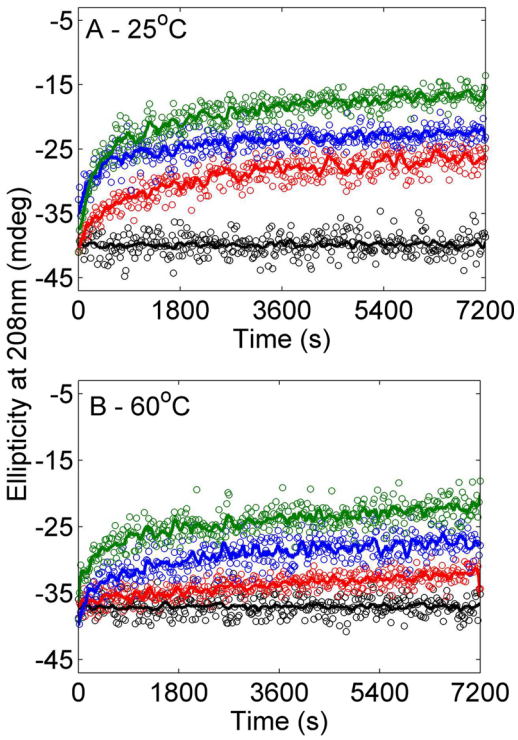

Figure 4. Kinetics of zinc-induced aggregation. Time course CD measurements were performed at 208 nm. The measurements that were started right after addition of zinc at the indicated concentration (black, 0 μM; red, 20 μM; blue, 50 μM; green, 100 μM) were performed at (A) 25 and (B) at 60 °C for 2 h. The ellipticity values were subtracted from those recorded under the same conditions but in the absence of BTL2 and smoothed using the Savitzky−Golay method.

noticeable changes for 2 h (Figure S2 of the Supporting Information), we observed gradual loss of ellipticity at both wavelengths for 20, 50, and 100 μM zinc additions (Figure 4A), in which the rate of aggregation was increased with an increasing zinc concentration (Table SI of the Supporting Information). Parallel to the observation above suggesting that an increasing zinc concentration hastens aggregation, a higher zinc concentration (50 μM) led to a profound decrease in the amount of soluble protein at 25 °C, yielding fainter protein bands on the SDS−PAGE gel (Figure 5B) compared with that at a lower zinc concentration (20 μM) (Figure 5A).

Effect of Temperature on the Zinc-Induced Aggregation. To assess the impact of temperature on the secondary structure of zinc-induced aggregates, we recorded the far-UV CD spectra for every 10 °C interval in the range of 30−90 °C (Figure 6A). The control BTL2 showed a gradual destabilization in the far-UV CD signals at 208 and 222 nm (Figure 6A and Figure S3 of the Supporting Information). In particular, the magnitudes of the signals at 208 nm (Figure S3 of the Supporting Information) and 222 nm (Figure 6A) reached the highest levels at 30 °C, gradually decreased from 30 to 60 °C, and reached the lowest level at 90 °C. The sample preincubated at 5 μM zinc produced results very similar to those of control BTL2. However, in contrast to the control and the 5 μM zinc preincubated samples, the samples incubated in the presence of ≥10 μM zinc did not display gradual destabilization in the CD signals such that the 60 °C spectrum showed the strongest CD signals at 208 and 222 nm for BTL2 preincubated in 50 and 100 μM zinc (Figure 6A and Figure S3 of the Supporting Information).

DOI: 10.1021/acs.biochem.5b00200
Biochemistry 2015, 54, 3901−3910

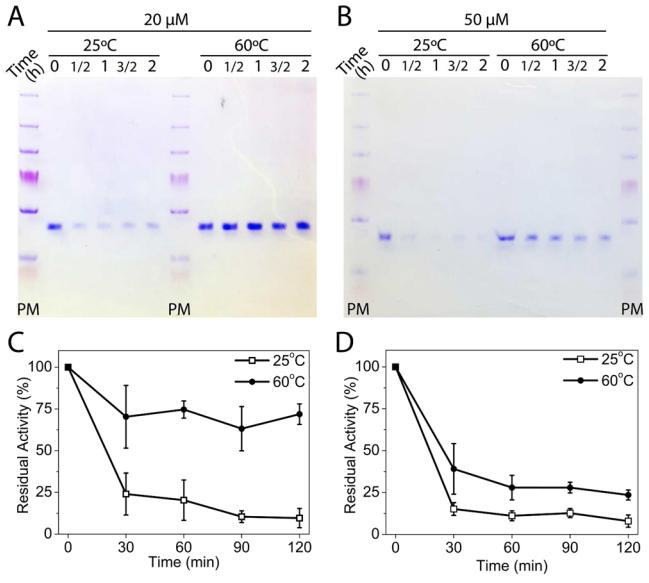

Figure 5. Solubility and activity analyses of the aggregates. Aggregation was induced by (A) 20 and (B) 50 μM zinc at 25 and 60 °C. Each mixture was sampled every 30 min and centrifuged before gel loading. The same samples loaded onto SDS–PAGE gels were analyzed in kinetic lipase assays. The percents of residual activity of soluble BTL2 in the aggregates formed at (C) 20 and (D) 50 μM zinc were represented by setting the activity of BTL2 before zinc addition to 100%.

Thermal denaturation of the native BTL2 resulted in a smooth profile with two distinct plateaus before and after denaturation at 222 nm, and similarly, BTL2 incubated at 5 μM zinc had the same denaturation curve as the native form (Figure 6B). However, when BTL2 was incubated at ≥10 μM zinc, we observed instead of a flat line, a distinct reduction in the CD intensity near the denaturation region (Figure 6B). Specifically, the denaturation curve of the 10 μM zinc incubation resulted in a curve overlapping with the native sample after 45 °C, and similarly the 50 μM zinc-preincubated sample yielded 222 nm signals that overlapped with that of native BTL2 at 65 °C (Figure 6B). On the other hand, the denaturation curve of the aggregates formed at 100 μM zinc lagged behind overlapping with the native curve, and showed only subtle reduction in the ellipticity at 65 °C (Figure 6B).

To assess the impact of temperature on the kinetics of zinc-induced aggregation, time course CD measurements were performed at different temperatures. The ellipticity at 208 nm did not show any changes at 25 and 60 °C for 2 h (Figure 4B), suggesting a stable structure for the control BTL2 throughout these measurements. Compared with the condition at 25 °C, the rates were reduced with increasing temperature regardless of zinc concentration used (Figure 4B and Table SI of the Supporting Information). The particular reduction in the aggregation rate at 60 °C was also inferred from the SDS–PAGE analysis in which the amount of soluble protein was increased gradually upon incubation at 60 °C (Figure 5A,B), clarifying the outcome that increased kinetic energy impedes with zinc-induced aggregation.

Impacts of Zinc on Thermal Denaturation. Thermal denaturation was profiled by monitoring the CD signals at 222 nm (Figure 6B). The melting temperatures (T_m) are listed in Table SII of the Supporting Information. Similar to the previous result,[17] the T_m of native BTL2 was found to be 73 °C at 222 nm, while the zinc-induced aggregates did not have any significant impact on the T_m. We have also performed thermal denaturation at a slower rate (2 °C/min) for the control and the sample preincubated at 5 μM zinc (Figure S4 of the Supporting Information). Although the T_m values of these conditions were slightly lower than those measured at a heating speed of 6 °C/min, the T_m values obtained from slow heating

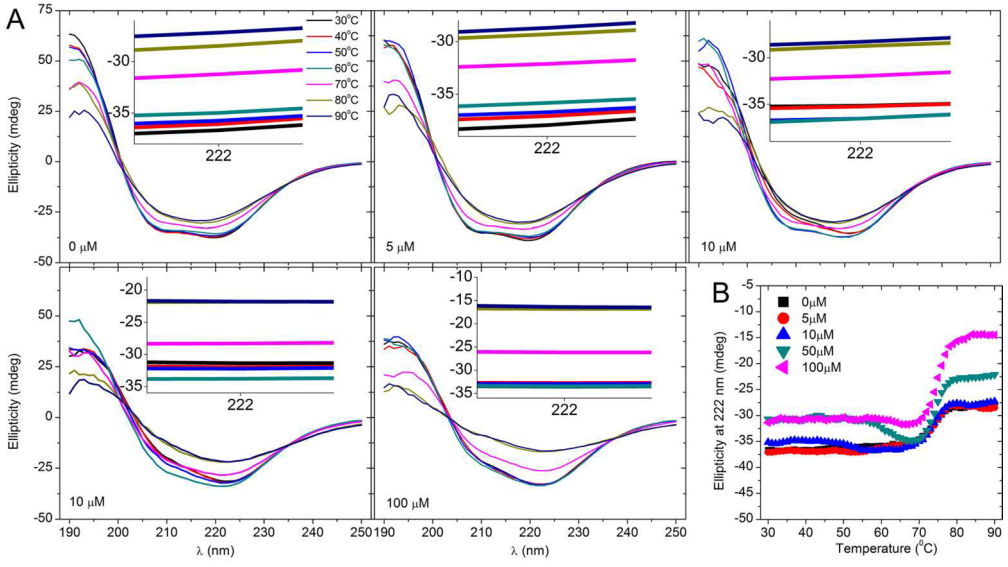

Figure 6. Thermal denaturation profiles. (A) Far-UV CD spectra of BTL2 at 10 μm preincubated in the presence of 0–100 μM zinc at different temperatures. The small rectangle marks the 222 nm region that is a characteristic signal for the BTL2 fold,[53] and the inset shows the CD intensity around this region. For all parts, the spectra are colored according to the measurement temperature: black, 30 °C; red, 40 °C; blue, 50 °C; cyan, 60 °C; pink, 70 °C; yellow, 80 °C; navy, 90 °C. (B) Denaturation profiles of BTL2 incubated at 0–100 μM zinc at 222 nm. The profiles shown here were obtained after subtracting the ellipticity of buffer solutions recorded at the indicated zinc concentration and in the absence of BTL2. See the Supporting Information for high-tension voltage data (Figure S10 of the Supporting Information) for the assessment of light scattering during measurements.

DOI: 10.1021/acs.biochem.5b00200
Biochemistry 2015, 54, 3901–3910

did not differ from those obtained from fast heating in both the control and the zinc-preincubated sample, suggesting that zinc-induced aggregation does not affect the thermodynamic stability of BTL2. We also monitored the CD signals at 222 nm upon cooling of the same samples at a rate of 2 °C/min, yet none of the conditions was able to restore native secondary structure upon cooling, suggesting that thermal unfolding of control BTL2 and zinc-induced BTL2 aggregates is irreversible. Lastly, zinc-free BTL2 showed a drastic decrease (~10 °C) in T_m (Figure S5 and Table SII of the Supporting Information), a result that agrees with the previous observations regarding zinc's involvement in the structural stability of thermoalkalophilic lipases.[34,40]

Functional Analysis of the Zinc-Induced Aggregates. To assess the lipase activity during zinc-induced aggregation, the samples analyzed in the kinetic analysis (Figures 4 and 5A,B) were used in lipase assays. The control BTL2 did not show any changes in the activity regardless of the incubation temperature (Figure S6 of the Supporting Information), showing that BTL2 preserved its function at 25 and 60 °C upon incubation for 2 h. At 25 °C, additions of 20 and 50 μM zinc significantly reduced the lipase activity to 25 and 15%, respectively (Figure 5C), which was restored to 75 and 40%, respectively, upon incubation at 60 °C (Figure 5D). We also assayed the residual lipase activity of the zinc-induced aggregates after incubation for 1 h at 60 °C. At 10 μM, BTL2 aggregates were able to restore almost all of the total activity upon thermal incubation for 1 h at 60 °C (Figure 7),

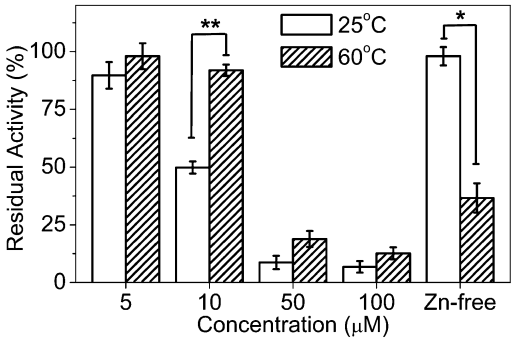

Figure 7. The residual activity of soluble BTL2 that was dissociated from the 2 h old aggregates upon incubation for 1 h at 25 or 60 °C. The percent activity was obtained by setting the activity of BTL2 in the absence of zinc to 100%. Statistical significance was determined with a Student's t test: $*p < 0.05$, and $**p < 0.01$ ($n = 3$).

similar to what we have observed during thermal denaturation of these aggregates that produced overlapping signals with the native structure at 60 °C (Figure 6B). On the other hand, the aggregates formed at high zinc concentrations (50 or 100 μM) showed only a slight increase in activity upon incubation at 60 °C (Figure 7). We last recorded the residual activity of zinc-free BTL2 and reported that zinc removal significantly reduced the lipase's stability at 60 °C by reducing the residual activity more than 50% (Figure 7).

DISCUSSION

Zinc Is Required for Dimerization and Thermostability. Initially, a DLS analysis was performed to assess the sizes of BTL2 molecules in response to the addition and removal of zinc. The intensity distribution is the fundamental size distribution that can be obtained from a DLS measurement; however, a realistic size description was not possible from our intensity distributions (Figure S7 of the Supporting Information). Although the samples were filtered prior to analysis, we could not eliminate the presence of large aggregates in the control BTL2, which interfered with the accurate determination of the sizes from intensity distributions. Such large aggregated particles, even if they are at negligible quantities, may comprise a significant portion of the scattered intensity because they scatter light proportional to the sixth power of their sizes. Hence, even in small portions, the presence of large particles may lead to inconclusive results in intensity size distributions (Figure S7 of the Supporting Information). This phenomenon has been previously encountered for another aggregation-prone protein,[41] in which the intensity distribution was converted to a volume distribution by the application of Mie's theory.[35] In line with this example, we also relied on the volume size distributions (Figure 1) by which we were able to obtain a fair description of BTL2 sizes showing that the large aggregated particles correspond to only a negligible portion of the total particles (<4%).

The 7 nm peak observed for the control BTL2 is in agreement with the size of dimer structures belonging to thermoalkalophilic lipases,[19−22] indicating that BTL2 adopted the dimeric form. On the other hand, chelation of zinc from the control BTL2 disrupted the dimer and led to formation of the monomer with an apparent radius of 3.6 nm[5,17] (Figure 1), accentuating the zinc's necessity for dimerization of BTL2. Moreover, upon incubation at varying zinc concentrations, BTL2 formed large aggregates (Figure 1). Overall DLS analysis basically indicated a link between zinc and self-assembly of BTL2, and thus a role for zinc in mediating the intermolecular interactions within the dimer and aggregates.

It has been postulated by the works of Choi et al.[34] and Bertoldo et al.[40] that zinc is essential for thermostability of the thermoalkalophilic lipases from *B. stearothermophilus* and *Staphylococcus xylosus* at elevated temperatures. In this study, we similarly found that the zinc-free BTL2 led to a reduction in the thermostability (50%) (Figure 7) and in T_m (~10 °C) of BTL2 (Table SII of the Supporting Information), agreeing with the previous findings for other thermoalkalophilic lipases.[34,40] These findings would point out that the presence of zinc at the coordination site is essential for the lipase to stabilize itself at high temperatures. The presence of such intramolecular metal coordination sites is a known factor that contributes to the thermostability of proteins.[19,34,40] However, in the light of our findings indicating a contribution of zinc to the dimerization of BTL2, we identify new factors that might also play critical roles in the thermostability of thermoalkalophilic lipases such as an increased number of intermolecular interactions[42−46] and increased surface area buried upon oligomerization.[47,48]

Possible Molecular Machinery behind Zinc-Mediated Dimerization. Despite being a rare metal for lipases,[23] structural studies marked a zinc coordination site in thermoalkalophilic lipases.[19−22,49] Essentially, the proximity of the zinc ion to the dimer interface (Figure 8A) prompted us to delineate the role of zinc in the self-assembly in thermoalkalophilic lipases. The zinc binding site in which two histidines (H81 and H87) and two aspartates (D61 and D238) coordinate zinc is shown in the L1 thermoalkalophilic lipase dimer (Figure 8A) that has a sequence 90% identical with that of BTL2. Zinc coordination joins three distant regions of the polypeptide chain, explicitly the 3_{10} helix (H81−H87), residues D61 and D238, in a structural domain (Figure 8B). Although

DOI: 10.1021/acs.biochem.5b00200
Biochemistry 2015, 54, 3901−3910

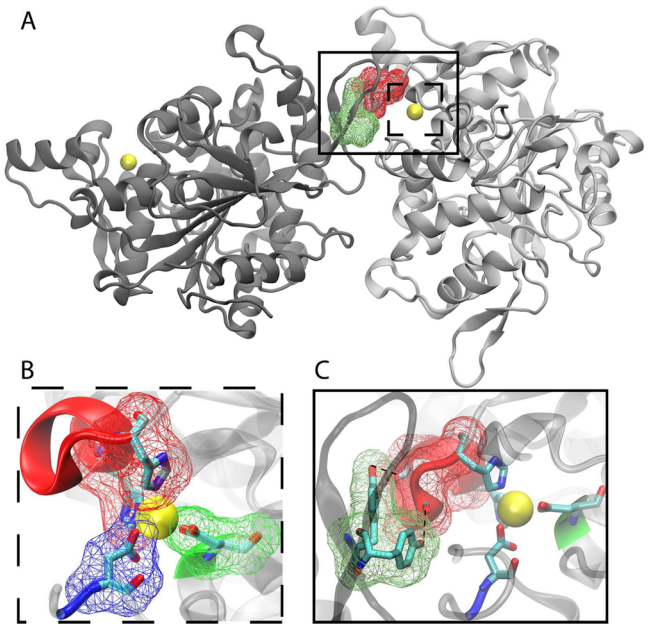

Figure 8. Zinc domain and intermolecular interactions at the dimer interface. (A) Crystal structure (PDB entry 1KU0) of the thermoalkalophilic lipase homodimer shown as a cartoon with the consecutive monomers colored dark gray and gray. The dashed rectangle represents the zinc domain (B) in which zinc-coordinating residues (H81, H87, D61, and D238) are rendered in wireframe and stick models (C, cyan; O, red; N, blue). The dimer interface is framed by a solid line in panel C where two intermolecular hydrogen bonds formed between the side chain hydroxyl groups of Y273 and Y282 of one subunit and the backbone carbonyl groups of A83 and H85 of the other subunit are marked with dashed black lines. The zinc ion is shown as a yellow van der Waals sphere for all parts.

zinc coordination is entirely intramolecular, the 3_{10} helix (H81−H87), which carries two zinc-coordinating histidines, has been shown to contribute to dimer interactions in a computational study,[17] in which the backbone carbonyl groups of A83 and H85 in the helix formed persistent hydrogen bonds with the side chain hydroxyl groups of Y273 and Y282 of the adjacent monomer (Figure 8C). Such structural zinc sites close to subunit interfaces have recently been associated with dimerization processes of other proteins in which interactions of zinc with the coordination site induce the formation of dimers.[50−52] Similarly, our findings about the zinc's role in the self-assembly of BTL2 indicated a direct contribution of zinc to the intermolecular interactions. Hence, along with the proximity of structural zinc to the dimer interface, the additional involvement of the zinc domain, particularly the 3_{10} helix (H81−H87), in the dimer interactions implies that zinc coordination is critical not only to formation of an intramolecular zinc domain (Figure 8B) but also to formation of the dimer (Figure 8C). Even though there was not any physical or structural evidence illustrating the molecular mechanism behind zinc's involvement in dimerization process of thermoalkalophilic lipases, in light of structural insights described above, we propose that the contribution of 3_{10} helix of the zinc domain to the dimer interactions (Figure 8C) would in part unveil the molecular machinery behind zinc-induced dimerization.

Zinc Induces Native-like Aggregation, Possibly through the Dimer Interface. Thermoalkalophilic lipases, including BTL2, possess the α/β hydrolase fold,[53] which was previously shown to give two characteristic bands at 208 and 222 nm in the far-UV CD spectrum.[17,34,40] Parallel to these observations, the far-UV CD spectrum of the control BTL2 indicated the characteristic hydrolase fold (Figure 2). Although 5 μM zinc induced formation of BTL2 aggregates with an apparent radius of 24 nm (Figure 1), far-UV CD spectra of these aggregates also agreed that they preserved native BTL2 structures (Figure 2). Aggregation in its conventional definition might refer to irreversible self-assembly of partially or fully unfolded protein structures;[54] however, zinc-induced aggregation of BTL2 should be termed "native-like aggregation", because of the finding that the aggregates exhibited native-like far-UV CD signals (Figure 2). On the other hand, the far-UV CD spectra of BTL2 preincubated in the presence of higher zinc concentrations (50−100 μM) led a distinct reduction in CD intensity, particularly for 208 nm (Figure 2). Curtailing CD signals would be likely to be due to excess light scattering from the aggregates, an outcome previously observed for another aggregation-prone protein.[41,55] In line with this concept, the lowest-intensity signals at 208 nm from 50 and 100 μM zinc incubations might imply a dramatic increase in the scattered light and thus in the amount of aggregate compared with the incubations performed at low zinc concentrations (5 and 10 μM).

Along with distinct light scatter at 208 nm, our findings further indicated separation of the characteristics between the aggregates formed at low and high zinc concentrations. Specifically, the aggregates that were formed at 5−10 μM zinc were soluble (Figure S8A of the Supporting Information), while those formed at higher zinc concentrations such as 50 or 100 μM were insoluble (Figure S8A of the Supporting Information) with apparent binding affinities toward Congo red and ThT (Figure 3 and Figure S1 of the Supporting Information). Such distinct biochemical features might indicate different aggregate forms representing different stages of the aggregation process.[26] The kinetic analysis revealed that aggregation was much faster at 50 μM zinc than it was at 10 μM zinc (Figure 4 and Figure S3 of the Supporting Information), suggesting that using a fixed incubation time, the aggregates formed at low zinc supplies would represent the early stages of the process while those formed at high zinc would represent the late stages. In this respect, we considered the aggregates formed in 2 h at low zinc concentrations ($\leq$10 μM) as the early aggregates and those formed at high concentrations ($\geq$50 μM) as the late aggregates. Another notable point is that the early aggregates obtained upon incubation at 10 μM zinc for 2 h turned into late aggregates in 12 h such that the aggregates formed in 12 h at 10 μM zinc were insoluble (Figure S8B of the Supporting Information) and able to bind Congo red with altered far-UV spectra (not shown). Clearly, both the concentration and the time-dependent formation of the zinc-induced aggregates allow us to obtain the late aggregates by incubating BTL2 at a high zinc concentration (50 μM) for 2 h or at a low zinc concentration (10 μM) for 12 h, suggesting the early aggregates as a metastable form of the zinc-induced aggregates.

Numerous proteins convert into amyloid-like fibrils and show common characteristics, including binding affinities for dyes like Congo red and ThT.[36,41] Although the early aggregates did not show binding affinity for Congo red or ThT, the late aggregates, those formed at high zinc concentrations, showed binding to these dyes (Figure 3 and Figure S1 of the Supporting Information), indicating that the

DOI: 10.1021/acs.biochem.5b00200
Biochemistry 2015, 54, 3901−3910

late insoluble aggregates might be in fibrillar form. Despite the fact that amyloid fibrils often possess extensive cross β-sheet structures,[36,41,56,57] the far-UV CD spectra of zinc-induced BTL2 aggregates are shown; those formed at low or high zinc concentrations did not show any β-sheet formation. Instead, they possessed similar CD signals, particularly at 222 nm with the control BTL2 (Figure 2), indicating native-like secondary structure in the zinc-induced aggregates. Considering recent evidence that has revealed that proteins that have native-like structural elements without any cross β-sheet structures may still form fibrillar aggregates,[58,59] we envision that the late insoluble aggregates might be in fibrillar form. Still accurate determination of the fibrillar morphology in the late aggregates should be performed through methods such as electron microscopy and/or atomic force microscopy,[60] steps that were not investigated in this study.

The findings for the early aggregates showing that they preserved native-like structures (Figure 2) and detached into native-like structures with lipase function by temperature changes (Figures 2 and 7) indicated that the early aggregates would have a defined binding interface to be packed in such ordered structures such as oligomers. This assertion was further bolstered by the SDS−PAGE analysis of the soluble zinc-induced aggregates in which two large proteins having approximate sizes of 90 and 130 kDa, along with the monomer (43 kDa), have been spotted corresponding to the dimer and the trimer BTL2, respectively (Figure S8B of the Supporting Information), showing that the soluble aggregates degraded into small BTL2 oligomers such as dimers (Figure S8B of the Supporting Information). Taken together with the structural insights into the ability of the lipase dimer to grow ordered aggregates through the dimer interface, we point out that the native-like zinc-induced aggregates might employ the dimer interface as their interaction surface.

Zinc-Induced Intermolecular Interactions Are Mediated by Temperature Switches. According to temperature-dependent analysis, the aggregation rate was slowed at elevated temperatures (Figure 4 and Table SI of the Supporting Information), indicating the high temperatures impair zinc-induced aggregation. Moreover, the loss of CD intensity due to light scattering rooted from zinc-induced aggregates can be almost fully regained at high temperatures, particularly for the early aggregates (Figures 4 and 6). In other words, curtailing of CD intensity due to light scattering in the presence of zinc-induced aggregates disappeared at high temperatures. Functional analysis also showed that the lipase activity can be substantially restored from the early aggregates, while the restoration of activity is limited for the aggregates formed at high zinc concentrations (Figure 7).

Larger proteins are more resistant to degradation and denaturation than smaller ones.[46] Despite the observation that T_m was not altered by the presence of zinc-induced aggregates (Table SII of the Supporting Information), reversible formation of the early zinc-induced aggregates might be considered as a thermostability strategy, analogous to the condition observed for zinc-induced BTL2 dimers. Because of the intermolecular interactions within the ordered aggregates, the lipase could resist temperatures higher than those resisted by nonaggregated forms.[43,45] Thus, reversible formation of the zinc-induced aggregates, as in oligomerization, could be considered as a thermostability strategy. Overall, we explain that BTL2 molecules can self-assemble through interactions mediated by zinc, which can be substantially reversed by an increased kinetic energy in the early stages of zinc-induced aggregation, while in the late stages the reversibility is compromised.

The observations described above also suggested that the reversible interactions within the early aggregates would undergo structural rearrangements in which the interactions in the late aggregates become irreversible and could no longer be solubilized by temperature switches. Such changes in the intermolecular interactions of the late aggregates, observed for other fibrillar aggregates,[26] might be used to support the hypothesis stating that the late aggregates form fibrillar structures.

CONCLUSIONS

Here we identified a role for zinc in the self-assembly of BTL2 in which the zinc-induced self-assemblies of BTL2, including the dimeric form, possess a thermostability advantage over the monomeric state. Despite zinc being an uncommon metal for lipases, apparently the preference of this lipase family for a structural zinc site at the dimer interface has a consequence for oligomerization and aggregation that has a consequence for thermostability. By the availability of the structural data, we also attempted to address a molecular basis for the zinc-induced dimerization that might be used to reveal critical positions for mutagenesis studies to fine-tune aggregation tendency and also stability. Finally, these findings might contribute to understanding of aggregation processes in which instead of an extensive search for misfolded or unfolded intermediates, native-like conformations can present candidate conformations for aggregation processes that occur naturally in thermophiles.

ASSOCIATED CONTENT

Supporting Information

Two tables of kinetic constants of aggregation and melting temperatures and 10 figures showing fluorescence micrographs, details of DLS, CD measurements, and solubility analysis. The Supporting Information is available free of charge on the ACS Publications website at DOI: 10.1021/acs.biochem.5b00200.

AUTHOR INFORMATION

Corresponding Author

*E-mail: emeld@sabanciuniv.edu. Telephone: +90 216 510 6653.

Funding

This work is supported by Türkiye Bilimsel ve Teknolojik Arastirma Kurumu (TUBITAK) 112T901.

Notes

The authors declare no competing financial interest.

ABBREVIATIONS

BTL2, *B. thermocatenulatus* lipase 2; CD, circular dichroism; DLS, dynamic light scattering; MRE, mean residue ellipticity; ThT, thioflavin T; T_m, melting temperature; TPEN, *N*,*N*,*N*′,*N*′-tetrakis(2-pyridylmethyl)ethylenediamine.

REFERENCES

(1) Schmid, R. D., and Verger, R. (1998) Lipases: Interfacial Enzymes with Attractive Applications. *Angew. Chem., Int. Ed. 37*, 1608−1633.

(2) Castro-Ochoa, L. D., Rodríguez-Gómez, C., Valerio-Alfaro, G., and Oliart Ros, R. (2005) Screening, purification and characterization

DOI: 10.1021/acs.biochem.5b00200
Biochemistry 2015, 54, 3901−3910

of the thermoalkalophilic lipase produced by *Bacillus thermoleovorans* CCR11. *Enzyme Microb. Technol. 37*, 648−654.
(3) Jeong, S. T., Kim, H. K., Kim, S. J., Pan, J. G., Oh, T. K., and Ryu, S. E. (2001) Crystallization and preliminary X-ray analysis of a thermoalkalophilic lipase from *Bacillus stearothermophilus* L1. *Acta Crystallogr. D57*, 1300−1302.
(4) Rua, M. L., Schmidt-Dannert, C., Wahl, S., Sprauer, A., and Schmid, R. D. (1997) Thermoalkalophilic lipase of *Bacillus thermocatenulatus* large-scale production, purification and properties: Aggregation behaviour and its effect on activity. *J. Biotechnol. 56*, 89−102.
(5) Schlieben, N. H., Niefind, K., and Schomburg, D. (2004) Expression, purification, and aggregation studies of His-tagged thermoalkalophilic lipase from *Bacillus thermocatenulatus*. *Protein Expression Purif. 34*, 103−110.
(6) Wang, W., and Roberts, C. J. (2010) *Aggregation of therapeutic proteins*, Wiley, Hoboken, NJ.
(7) Hamrang, Z., Rattray, N. J., and Pluen, A. (2013) Proteins behaving badly: Emerging technologies in profiling biopharmaceutical aggregation. *Trends Biotechnol. 31*, 448−458.
(8) Ross, C. A., and Poirier, M. A. (2004) Protein aggregation and neurodegenerative disease. *Nat. Med. 10* (Suppl.), S10−S17.
(9) Ciryam, P., Tartaglia, G. G., Morimoto, R. I., Dobson, C. M., and Vendruscolo, M. (2013) Widespread aggregation and neurodegenerative diseases are associated with supersaturated proteins. *Cell Rep. 5*, 781−790.
(10) Ross, C. A., and Poirier, M. A. (2005) Opinion: What is the role of protein aggregation in neurodegeneration? *Nat. Rev. Mol. Cell Biol. 6*, 891−898.
(11) Dünhaupt, A., Lang, S., and Wagner, F. (1992) *Pseudomonas cepacia* lipase: Studies on aggregation, purification and on the cleavage of olive oil. *Biotechnol. Lett. 14*, 953−958.
(12) Lesuisse, E., Schanck, K., and Colson, C. (1993) Purification and preliminary characterization of the extracellular lipase of *Bacillus subtilis* 168, an extremely basic pH-tolerant enzyme. *Eur. J. Biochem. 216*, 155−160.
(13) Sztajer, H., Lunsdorf, H., Erdmann, H., Menge, U., and Schmid, R. (1992) Purification and properties of lipase from *Penicillium simplicissimum*. *Biochim. Biophys. Acta 1124*, 253−261.
(14) Sugihara, A., Tani, T., and Tominaga, Y. (1991) Purification and Characterization of a Novel Thermostable Lipase from *Bacillus* sp. *J. Biochem. 109*, 211−216.
(15) Jaeger, K.-E., Adrian, F.-J., Meyer, H. E., Hancock, R. E. W., and Winkler, U. K. (1992) Extracellular lipase from *Pseudomonas aeruginosa* is an amphiphilic protein. *Biochim. Biophys. Acta 1120*, 315−321.
(16) Schmidt-Dannert, C., Sztajer, H., Stocklein, W., Menge, U., and Schmid, R. D. (1994) Screening, purification and properties of a thermophilic lipase from *Bacillus thermocatenulatus*. *Biochim. Biophys. Acta 1214*, 43−53.
(17) Timucin, E., and Sezerman, O. U. (2013) The conserved lid tryptophan, W211, potentiates thermostability and thermoactivity in bacterial thermoalkalophilic lipases. *PLoS One 8*, e85186.
(18) Salameh, M. A., and Wiegel, J. (2010) Effects of Detergents on Activity, Thermostability and Aggregation of Two Alkalithermophilic Lipases from *Thermosyntropha lipolytica*. *Open Biochem. J. 4*, 22−28.
(19) Jeong, S. T., Kim, H. K., Kim, S. J., Chi, S. W., Pan, J. G., Oh, T. K., and Ryu, S. E. (2002) Novel zinc-binding center and a temperature switch in the *Bacillus stearothermophilus* L1 lipase. *J. Biol. Chem. 277*, 17041−17047.
(20) Tyndall, J. D., Sinchaikul, S., Fothergill-Gilmore, L. A., Taylor, P., and Walkinshaw, M. D. (2002) Crystal structure of a thermostable lipase from *Bacillus stearothermophilus* P1. *J. Mol. Biol. 323*, 859−869.
(21) Matsumura, H., Yamamoto, T., Leow, T. C., Mori, T., Salleh, A. B., Basri, M., Inoue, T., Kai, Y., and Rahman, R. N. (2008) Novel cation-π interaction revealed by crystal structure of thermoalkalophilic lipase. *Proteins 70*, 592−598.
(22) Ruslan, R., Abd Rahman, R. N., Leow, T. C., Ali, M. S., Basri, M., and Salleh, A. B. (2012) Improvement of Thermal Stability via Outer-Loop Ion Pair Interaction of Mutated T1 Lipase from *Geobacillus zalihae* Strain T1. *Int. J. Mol. Sci. 13*, 943−960.
(23) Arpigny, J. L., and Jaeger, K. E. (1999) Bacterial lipolytic enzymes: Classification and properties. *Biochem. J. 343* (Part1), 177−183.
(24) Esler, W. P., Stimson, E. R., Jennings, J. M., Ghilardi, J. R., Mantyh, P. W., and Maggio, J. E. (1996) Zinc-induced aggregation of human and rat β-amyloid peptides in vitro. *J. Neurochem. 66*, 723−732.
(25) Huang, X., Atwood, C. S., Moir, R. D., Hartshorn, M. A., Vonsattel, J. P., Tanzi, R. E., and Bush, A. I. (1997) Zinc-induced Alzheimer's Aβ1−40 aggregation is mediated by conformational factors. *J. Biol. Chem. 272*, 26464−26470.
(26) Calabrese, M. F., and Miranker, A. D. (2009) Metal binding sheds light on mechanisms of amyloid assembly. *Prion 3*, 1−4.
(27) Faller, P. (2009) Copper and zinc binding to amyloid-β: Coordination, dynamics, aggregation, reactivity and metal-ion transfer. *ChemBioChem 10*, 2837−2845.
(28) Innocenti, M., Salvietti, E., Guidotti, M., Casini, A., Bellandi, S., Foresti, M. L., Gabbiani, C., Pozzi, A., Zatta, P., and Messori, L. (2010) Trace copper(II) or zinc(II) ions drastically modify the aggregation behavior of amyloid-β1−42: An AFM study. *J. Alzheimer's Dis. 19*, 1323−1329.
(29) Jobling, M. F., Huang, X., Stewart, L. R., Barnham, K. J., Curtain, C., Volitakis, I., Perugini, M., White, A. R., Cherny, R. A., Masters, C. L., Barrow, C. J., Collins, S. J., Bush, A. I., and Cappai, R. (2001) Copper and zinc binding modulates the aggregation and neurotoxic properties of the prion peptide PrP106−126. *Biochemistry 40*, 8073−8084.
(30) Miller, Y., Ma, B., and Nussinov, R. (2010) Zinc ions promote Alzheimer Aβ aggregation via population shift of polymorphic states. *Proc. Natl. Acad. Sci. U.S.A. 107*, 9490−9495.
(31) Majhi, P. R., Ganta, R. R., Vanam, R. P., Seyrek, E., Giger, K., and Dubin, P. L. (2006) Electrostatically driven protein aggregation: β-Lactoglobulin at low ionic strength. *Langmuir 22*, 9150−9159.
(32) Vogelsberg-Ragaglia, V., Bruce, J., Richter-Landsberg, C., Zhang, B., Hong, M., Trojanowski, J. Q., and Lee, V. M. (2000) Distinct FTDP-17 missense mutations in tau produce tau aggregates and other pathological phenotypes in transfected CHO cells. *Mol. Biol. Cell 11*, 4093−4104.
(33) Durmaz, E., Kuyucak, S., and Sezerman, U. O. (2013) Modifying the catalytic preference of tributyrin in *Bacillus thermocatenulatus* lipase through in-silico modeling of enzyme-substrate complex. *Protein Eng., Des. Sel. 26*, 325−333.
(34) Choi, W. C., Kim, M. H., Ro, H. S., Ryu, S. R., Oh, T. K., and Lee, J. K. (2005) Zinc in lipase L1 from *Geobacillus stearothermophilus* L1 and structural implications on thermal stability. *FEBS Lett. 579*, 3461−3466.
(35) Hulst, H. C. v. d. (1957) *Light scattering by small particles*, Wiley, New York.
(36) Nilsson, M. R. (2004) Techniques to study amyloid fibril formation in vitro. *Methods 34*, 151−160.
(37) Voropai, E. S., Samtsov, M. P., Kaplevskii, K. N., Maskevich, A. A., Stepuro, V. I., Povarova, O. I., Kuznetsova, I. M., Turoverov, K. K., Fink, A. L., and Uverskii, V. N. (2003) Spectral Properties of Thioflavin T and Its Complexes with Amyloid Fibrils. *J. Appl. Spectrosc. 70*, 868−874.
(38) Humphrey, W., Dalke, A., and Schulten, K. (1996) VMD: Visual molecular dynamics. *J. Mol. Graphics 14*, 33−38.
(39) LeVine, H., III (1999) Quantification of β-sheet amyloid fibril structures with thioflavin T. *Methods Enzymol. 309*, 274−284.
(40) Bertoldo, J. B., Razzera, G., Vernal, J., Brod, F. C., Arisi, A. C., and Terenzi, H. (2011) Structural stability of *Staphylococcus xylosus* lipase is modulated by Zn^{2+} ions. *Biochim. Biophys. Acta 1814*, 1120−1126.
(41) Plakoutsi, G., Taddei, N., Stefani, M., and Chiti, F. (2004) Aggregation of the Acylphosphatase from *Sulfolobus solfataricus*: The folded and partially unfolded states can both be precursors for amyloid formation. *J. Biol. Chem. 279*, 14111−14119.

DOI: 10.1021/acs.biochem.5b00200
Biochemistry 2015, 54, 3901−3910

(42) Ali, M. H., and Imperiali, B. (2005) Protein oligomerization: How and why. *Bioorg. Med. Chem. 13*, 5013−5020.
(43) Merkler, D. J., Srikumar, K., Marchese-Ragona, S. P., and Wedler, F. C. (1988) Aggregation and thermo-inactivation of glutamine synthetase from an extreme thermophile, *Bacillus caldolyticus*. *Biochim. Biophys. Acta 952*, 101−114.
(44) Salminen, T., Teplyakov, A., Kankare, J., Cooperman, B. S., Lahti, R., and Goldman, A. (1996) An unusual route to thermostability disclosed by the comparison of *Thermus thermophilus* and *Escherichia coli* inorganic pyrophosphatases. *Protein Sci. 5*, 1014−1025.
(45) Tanaka, Y., Tsumoto, K., Yasutake, Y., Umetsu, M., Yao, M., Fukada, H., Tanaka, I., and Kumagai, I. (2004) How oligomerization contributes to the thermostability of an archaeon protein. Protein L-isoaspartyl-O-methyltransferase from *Sulfolobus tokodaii*. *J. Biol. Chem. 279*, 32957−32967.
(46) Walden, H., Bell, G. S., Russell, R. J., Siebers, B., Hensel, R., and Taylor, G. L. (2001) Tiny TIM: A small, tetrameric, hyperthermostable triosephosphate isomerase. *J. Mol. Biol. 306*, 745−757.
(47) Haney, P., Konisky, J., Koretke, K. K., Luthey-Schulten, Z., and Wolynes, P. G. (1997) Structural basis for thermostability and identification of potential active site residues for adenylate kinases from the archaeal genus *Methanococcus*. *Proteins 28*, 117−130.
(48) Stellwagen, E., and Wilgus, H. (1978) Relationship of protein thermostability to accessible surface area. *Nature 275*, 342−343.
(49) Carrasco-Lopez, C., Godoy, C., de Las Rivas, B., Fernandez-Lorente, G., Palomo, J. M., Guisan, J. M., Fernandez-Lafuente, R., Martinez-Ripoll, M., and Hermoso, J. A. (2009) Activation of bacterial thermoalkalophilic lipases is spurred by dramatic structural rearrangements. *J. Biol. Chem. 284*, 4365−4372.
(50) Chi, Y. I., Sadler, I., Jablonski, L. M., Callantine, S. D., Deobald, C. F., Stauffacher, C. V., and Bohach, G. A. (2002) Zinc-mediated dimerization and its effect on activity and conformation of staphylococcal enterotoxin type C. *J. Biol. Chem. 277*, 22839−22846.
(51) Kozin, S. A., Mezentsev, Y. V., Kulikova, A. A., Indeykina, M. I., Golovin, A. V., Ivanov, A. S., Tsvetkov, P. O., and Makarov, A. A. (2011) Zinc-induced dimerization of the amyloid-β metal-binding domain 1−16 is mediated by residues 11−14. *Mol. BioSyst. 7*, 1053−1055.
(52) Kozin, S. A., Kulikova, A. A., Istrate, A. N., Tsvetkov, P. O., Zhokhov, S. S., Mezentsev, Y. V., Kechko, O. I., Ivanov, A. S., Polshakov, V. I., and Makarov, A. A. (2015) The English (H6R) familial Alzheimer's disease mutation facilitates zinc-induced dimerization of the amyloid-β metal-binding domain. *Metallomics 7*, 422−425.
(53) Ollis, D. L., Cheah, E., Cygler, M., Dijkstra, B., Frolow, F., Franken, S. M., Harel, M., Remington, S. J., Silman, I., Schrag, J., et al. (1992) The α/β hydrolase fold. *Protein Eng. 5*, 197−211.
(54) Fink, A. L. (1998) Protein aggregation: Folding aggregates, inclusion bodies and amyloid. *Folding Des. 3*, R9−R23.
(55) Brazil, B. T., Ybarra, J., and Horowitz, P. M. (1998) Divalent cations can induce the exposure of GroEL hydrophobic surfaces and strengthen GroEL hydrophobic binding interactions. Novel effects of Zn^{2+} GroEL interactions. *J. Biol. Chem. 273*, 3257−3263.
(56) Khurana, R., Coleman, C., Ionescu-Zanetti, C., Carter, S. A., Krishna, V., Grover, R. K., Roy, R., and Singh, S. (2005) Mechanism of thioflavin T binding to amyloid fibrils. *J. Struct. Biol. 151*, 229−238.
(57) Nelson, R., Sawaya, M. R., Balbirnie, M., Madsen, A. O., Riekel, C., Grothe, R., and Eisenberg, D. (2005) Structure of the cross-β spine of amyloid-like fibrils. *Nature 435*, 773−778.
(58) Bousset, L., Thomson, N. H., Radford, S. E., and Melki, R. (2002) The yeast prion Ure2p retains its native α-helical conformation upon assembly into protein fibrils in vitro. *EMBO J. 21*, 2903−2911.
(59) Laurine, E., Gregoire, C., Fandrich, M., Engemann, S., Marchal, S., Thion, L., Mohr, M., Monsarrat, B., Michel, B., Dobson, C. M., Wanker, E., Erard, M., and Verdier, J. M. (2003) Lithostathine quadruple-helical filaments form proteinase K-resistant deposits in Creutzfeldt-Jakob disease. *J. Biol. Chem. 278*, 51770−51778.
(60) Xia, W., and Xu, H. (2005) *Amyloid precursor protein: A practical approach*, CRC Press, Boca Raton, FL.

DOI: 10.1021/acs.biochem.5b00200
Biochemistry 2015, 54, 3901−3910